

## Article

# Turbulence Characteristics in Mild and Steep Entrance Slopes of Pool-Riffle Sequences

Negar Soltani <sup>1</sup>, Hossein Afzalimehr <sup>2</sup>, Ehsan Shahiri Tabarestani <sup>2</sup>, Alireza Eftekhari <sup>2</sup>, Marzieh Khabari <sup>2</sup>, Mohammad Nazari-Sharabian <sup>3,\*</sup>  and Moses Karakouzian <sup>4</sup> 

<sup>1</sup> Department of Civil and Environmental Engineering, Pennsylvania State University, University Park, State College, PA 16802, USA

<sup>2</sup> School of Civil Engineering, Iran University of Science and Technology, Tehran 13114-16846, Iran

<sup>3</sup> Department of Mathematics, Engineering, and Computer Science, West Virginia State University, Institute, WV 25112, USA

<sup>4</sup> Department of Civil and Environmental Engineering and Construction, University of Nevada Las Vegas, Las Vegas, NV 89154, USA

\* Correspondence: m.nazari@wvstateu.edu

**Abstract:** This study investigates the distributions of velocity and Reynolds stress in an artificial pool-riffle sequence for two entrance slopes of 5° and 20° in a laboratory and compares the results with a similar pool-riffle sequence in a gravel-bed river in central Iran. Quadrant analysis is applied to find out the contributions of different events on turbulent flow structures. At an entrance slope of 5°, the velocity distribution follows an exponential trend without flow separation, but for the entrance slope of 20°, the velocity distribution indicates a S-shaped pattern with flow separation. Variation of entrance slope does not influence the convex form of Reynolds stress (RS) distribution, but it influences the location of the maximum value of RS and the flow separation zone length. The results reveal that outward and ejection are the dominant events for both field and laboratory settings. The sweep displays a decreasing trend from near the bed toward the water surface, however, the outward contribution indicates an increasing trend from the bed toward the water surface. The agreement between laboratory and field results in velocity and Reynolds stress will help the river engineers to better manage complex fluvial processes. Bursting process events depend on the aspect ratio for the same entrance pool slope. The agreement in the results of velocity and Reynolds stress distributions and the dominant events of bursting process in the laboratory and field are encouraging for better restoration of rivers and decreasing the cost of projects.

**Keywords:** bursting; gravel-bed rivers; pool riffle slopes; turbulent flow



**Citation:** Soltani, N.; Afzalimehr, H.; Tabarestani, E.S.; Eftekhari, A.; Khabari, M.; Nazari-Sharabian, M.; Karakouzian, M. Turbulence Characteristics in Mild and Steep Entrance Slopes of Pool-Riffle Sequences. *Water* **2023**, *15*, 720. <https://doi.org/10.3390/w15040720>

Academic Editor: Bommanna Krishnappan

Received: 29 December 2022

Revised: 27 January 2023

Accepted: 9 February 2023

Published: 11 February 2023



**Copyright:** © 2023 by the authors. Licensee MDPI, Basel, Switzerland. This article is an open access article distributed under the terms and conditions of the Creative Commons Attribution (CC BY) license (<https://creativecommons.org/licenses/by/4.0/>).

## 1. Introduction

In river engineering, most studies are conducted in lab-based experiments under controlled conditions [1–7]. The extension of the laboratory results to the field needs a simultaneous study to find out the rate of agreement in results under control conditions with those in rivers. Exact replication of river conditions, such as the irregular shape of the river bed and variation in sediment particle size inside an experiment, is nearly impossible, calling for a detailed study under controlled conditions on a laboratory scale. Pool and riffle sequences with different entrance and exit slopes are dominant bed forms in gravel-bed rivers [8]. Since the pool and riffle turbulence structures affect many aspects of fluvial hydraulics and roughness coefficient estimation, investigating pool-riffle sequences plays a significant role in river restoration projects. In addition, the changes in velocity and Reynolds stress along a bed form influence the estimation of hydraulic parameters [5,8,9].

In the pool entrance, the velocity declines, while the pressure gradient increases [9,10]. The flow becomes uniform in the middle of the bedform, where the bed is flat [9], and the maximum mean longitudinal and transverse velocities occur near the pool bed [5].

In the riffle area, the secondary flow occurs due to high turbulence near the bed and a separation zone in the pool region [8]. The favorable pressure gradient occurs in the riffle section at the exit slope of the bedform [9–11]. The simultaneous increase in the entrance slope and the flow separation zone length affects the mean and instantaneous velocity distributions, leading to a change in estimating the key parameters of fluvial hydraulics [3]. This change can considerably influence the application of hydraulic models in rivers. Fazel Najafabadi et al. [11] built two- and three-dimensional models of an artificial pool-riffle in a channel with a fixed width and investigated and compared the hydraulic characteristics of the flow, including velocity, Reynolds stress, and the occurrence of flow separation. They found a reasonable agreement between the laboratory and river results for two-dimensional flow. However, the laboratory results revealed lower velocity than that in rivers for three-dimensional flow. They found out that, in the presence of two-dimensional pool-riffle bedforms, the velocities in the direction of the flow near the bed are high on the upstream riffle bedform and decrease in the pool during the flow decelerating in this part. Since the pool and riffle turbulence structures affect many aspects of fluvial hydraulics and roughness coefficient estimation, investigating pool-riffle sequences plays a significant role in river restoration projects. Therefore, several researchers attempted to construct an artificial pool and riffle sequence in a laboratory to collect data with more exact conditions [3,12,13]. Velocity and Reynolds stress calculations and the quadrant analysis help us better understand the effect of turbulent structures in river dynamics and their interaction with pool and riffle [14].

Some studies show that, in the natural pool and riffle, the scales of coherent turbulent flow structures decrease with velocity and discharge and do not depend on morphological scaling [8]. According to [15], flow structure is influenced significantly by the sedimentation depth of the pool-riffle sequence in gravel-bed rivers. Soltani et al. [16] revealed that Reynolds stress and turbulence intensity for accelerating and decelerating flows along a reach follow a convex form in the main flow direction. Additionally, in the riffle section, the vertical velocity vectors orient toward the bed; however, the orientation of the vectors is downward near the bed and upward at higher levels for the pool section.

In general, for natural conditions, the flow and the bed are non-uniform. The non-uniformity causes the velocity and turbulence distributions to change along the stream, leading to changes in the estimation of key fluvial hydraulic parameters. The geometry of the pool and riffle, including the entrance and exit slopes, influence the velocity and turbulence distributions, calling for more research on the interaction of the flow and geometry in pool and riffle sequences.

Up to the present date, no general procedure has been established on how laboratory results should be applied to rivers.

Our understanding is only based on laboratory results, which may not be helpful to address river challenges because the findings under control conditions in the laboratory are not always transferrable to complex conditions in rivers. Considering the strict budget and significant risk to work in rivers, it is necessary to understand and compare the results of the field and laboratory to find out similar flow features. The achievement of this comparative study will help managers to know which hydraulic patterns, including velocity and Reynolds stress distributions, are independent of scale, so they can be applied in both laboratory and gravel-bed rivers.

This study investigates the turbulence features in an artificial pool-riffle sequence and compares the results with collected data with the results in a natural pool-riffle sequence in the Pelasjan River in central Iran for different entrance slopes. The objectives of this study are to investigate the following:

1. How do velocity and Reynolds stress values change in different entrance slopes of an artificial pool-riffle sequence?
2. What are the dominant events in the bursting process in mild slope ( $5^\circ$ ) and steep slope ( $20^\circ$ ) in an artificial natural pool-riffle sequence? Can the aspect ratio influence the contribution of each event?

- How much agreement exists between the results on a laboratory scale with those in a gravel-bed river?

## 2. Materials and Methods

### 2.1. Field Measurements

Field study aims to find out the geometry and hydraulic characteristics, which can easily be reproduced on a laboratory scale. Accordingly, the field study was conducted in the Pelasjan River (Figure 1), one of the branches of the Zayandehrood River in central Iran. The experiment location was selected after 56 km of walking along the river route and finding an appropriate, explicit, and secure reach regarding researchers' safety and the instruments' protection. River discharge was measured at the beginning of each day to determine the flow discharge variation during data collection. Since the flow discharge variation was insignificant, the flow was considered permanent during data collection with a rate of  $9.68 \frac{m^3}{s}$  [17]. Table 1 presents a summary of river data.  $d_{50}$  and  $d_{90}$  indicate that 50% and 90% of the particles in the study area are smaller than this, respectively; in the study area, the flow was subcritical (the Froude number was between 0.04 and 0.4). The relative submergence parameter,  $\frac{h}{d_{50}}$ , and the aspect ratio parameter,  $\frac{W}{h}$ , had mean and average values of 3.36 and 132.9, respectively (Table 1). The standard deviation of the particle size  $\sqrt{\frac{d_{84}}{d_{16}}}$  was 1.4, showing uniform particle distribution in the selected reach.



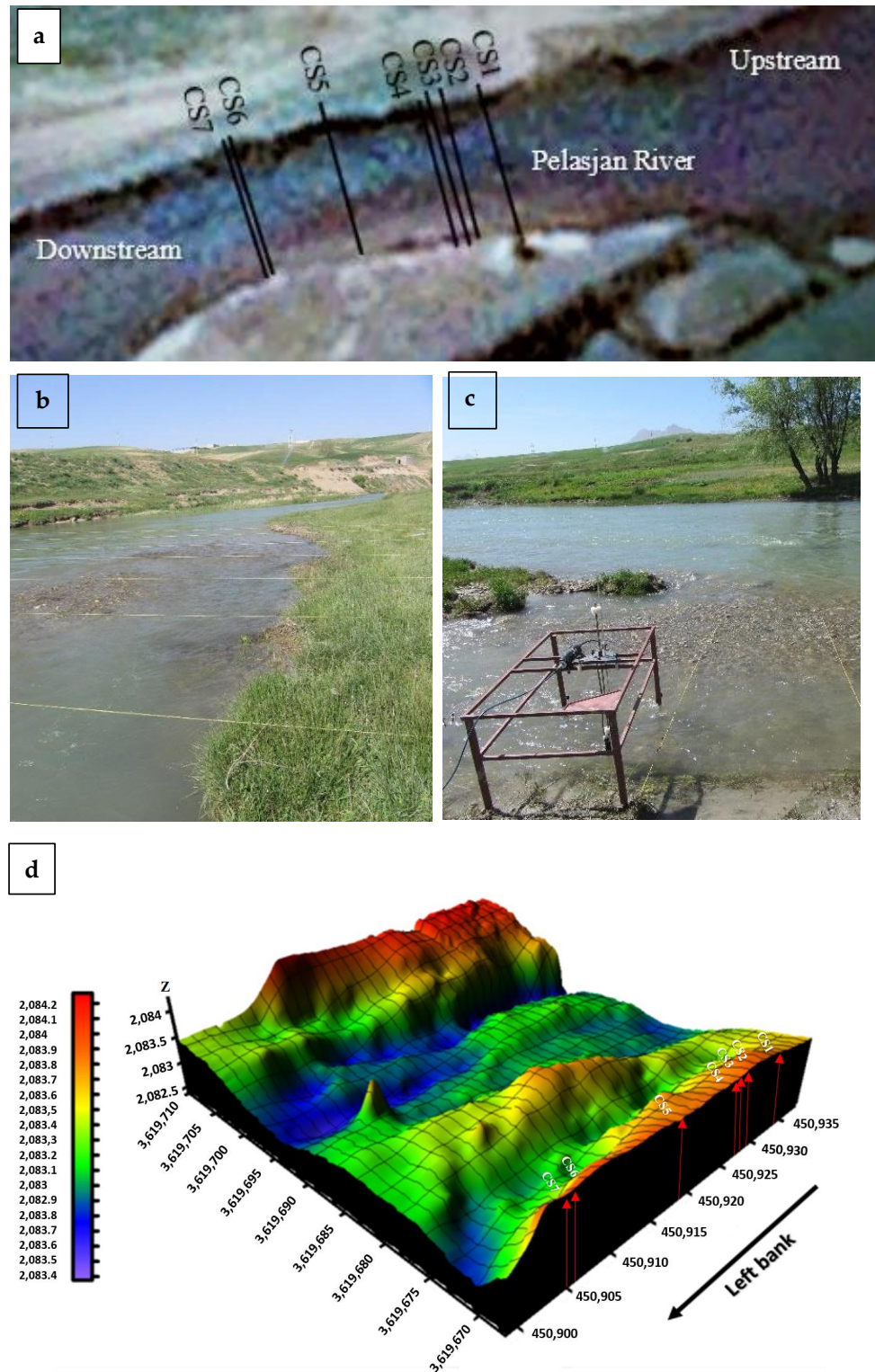
Figure 1. The location of the study area in the Pelasjan River.

Table 1. Geometric and hydraulic characteristics of the selected area in the Pelasjan River.

W (m)	h (m)	$d_{16}$ (cm)	$d_{50}$ (cm)	$d_{84}$ (cm)	$d_{90}$ (cm)	$\frac{h}{d_{50}}$	$\frac{W}{h}$	$\sigma$	Fr
49.2	0.37	10.4	11	17.5	21	3.36	132.9	1.39	0.19

As the first step in the data collection process, a Leica total station camera TC 1700 was used to determine the topography of the riverbed and riverbank with an accuracy of 1.7 s. The TC 17000 camera is used for land surveys and gathering geospatial data. This model has a dual compensator to correct tilt, and its minimum focusing distance is 1.5 to 4.5 m. The grid was made by pulling ropes in the desired area and completing a grid of 1 m in the longitudinal direction and 0.5 m in the transverse direction. Additionally, the riverbank was mapped at a distance of 1 m. Figure 2a shows the study area and cross-sections of the Pelasjan River. Figure 2b,c show how rectangular grid, mapping, and ADV data collection were conducted. Figure 2d also shows the topographic map of the selected bedform in

the river. WinADV delivers a domain for quantitatively analyzing the collected data using SonTek and Nortek acoustic Doppler velocimeters (ADV). WinADV can quickly view time series diagrams, histograms, or FFTs of the different velocity data.



**Figure 2.** (a) The selected reach and cross-sections of the Pelasjan River, (b) rectangular grid and mapping operations, (c) ADV deployment in the river to collect velocity data, and (d) topographic map of the Pelasjan River in the study area (in x, y, z direction, all units are meters).

This study used the Wolman method to determine the grain size distribution [17–20]. To use the ADV in the river, the device was placed on a sampling desk. The desk dimensions were  $1.5 \text{ m} \times 0.7 \text{ m}$ , and the heights of the stands were adjustable. The velocimeter was placed in the center of the sampling desk and attached to a triangular plate. This adjustment results in modifying the velocimeter position in the vertical direction and making it perform independently of the effect of the stands. The measurements were conducted with a sampling frequency of 200 Hz for 120 s, resulting in 24,000 data for each point in three directions. For the sampling volume, velocity measurements are performed at 50 mm from the transmitter in the center of a cylindrical volume with a fixed diameter of 6 mm, and the height is adjustable between 3 and 15 mm.

Kabiri et al. compared the difference in sampling velocity duration between 120 s and 300 s for 200 Hz frequency and concluded that the data collection for 120 s was suitable [21]. For data improvement, two modifications were performed, first, using the Goring and Nikora methods, and second, using the capabilities of WinADV software [22,23]. After measuring the point velocity, shear velocity and Reynolds stress were calculated along the pool-riffle sequence. To measure the flow depth, a mobile limimeter was used. The velocity components were measured three-dimensionally, and WinADV was considered for filtering data (minimum SNR > 15 and minimum correlation > 70). The grain size distribution and median grain size were obtained using the Wolman method. To find the longitudinal slope in the river, and to use it in laboratory experiments, the Surfer application was used to analyze data collected for river topography.

## 2.2. Laboratory Experiment

Experiments were conducted in a rectangular channel 16 m long, 90 cm wide, and 60 cm high with glass walls, a glass floor, and a bed slope of  $0^\circ$ . The collected sediment from the Pelasjan River was used as a cover for the laboratory flume bed. Next, the turbulent flow characteristics were measured on a sequence of pool-riffle with entrance and exit slopes of  $5^\circ$  and  $20^\circ$ , respectively (Figure 3). As presented in Table 2, this study led to three categories. Twenty-one profiles were taken in the flume entrance, with a discharge of  $40 \frac{\text{L}}{\text{s}}$ . The length of each part of the inlet and exit slopes, and the flat part of the bedform were taken 50 cm.

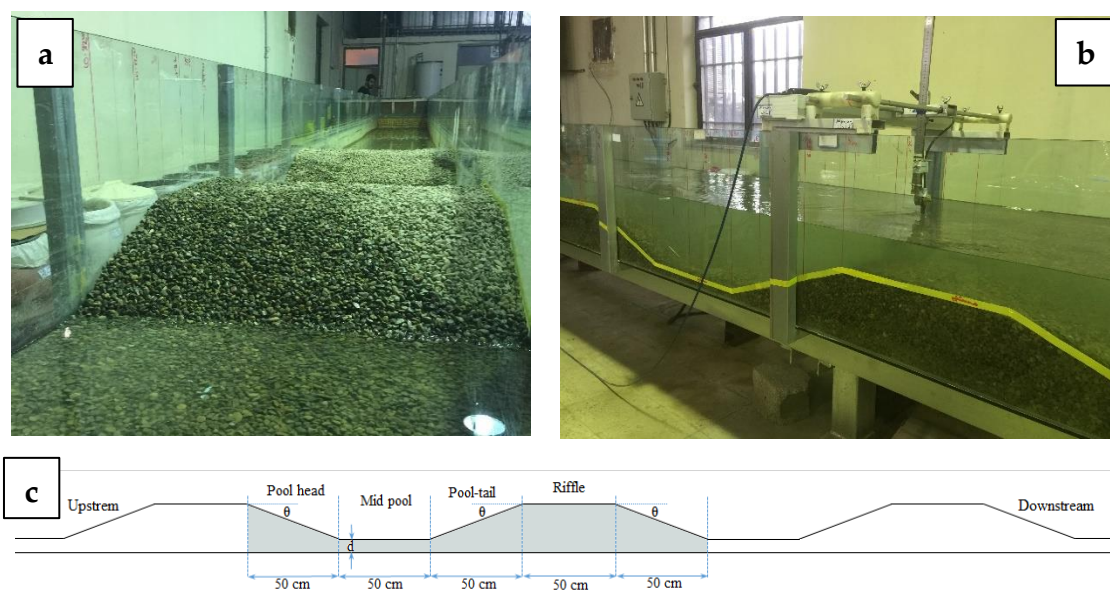


**Figure 3.** (a) Front view of the laboratory channel, (b) side view of the laboratory channel, and (c) schematic of the bed from upstream to downstream (shaded parts represent the length of the test area).

**Table 2.** Flow conditions in the laboratory flume.

Series	$\frac{W}{h}$	h (cm)	Slope (degree)
A	6	15	5
B	3.6	25	5
C	3	30	20

The turbulent flow structures were studied in the three series, as mentioned in Table 2. Compare the results of series A and B, showing the effect of aspect ratio greater than and less than five in the pool-riffle sequence on the results.

Compare the results of series B and C, showing the difference between entrance and exit slopes in the pool-riffle sequence when the rest of the hydraulic parameters were constant.

The following considerations were performed during preparing the laboratory setup: before constructing the bedform, the water depth in the pool part of the channel was 25 cm, and the aspect ratio ( $w/h$ ) was less than five. Profiles were taken in the center of the artificial bedform as series “a”.

In series “b”, the flow and experiment conditions were the same as in series “a,” the only difference being the flow depth. The flow depth in the pool area was 15 cm, and the aspect ratio was more than five.

In series “c,” an artificial pool and riffle bedform were created with entrance and exit angles of  $20^\circ$ , at 8 m from the flume’s most substantial upstream location with a maximum flow depth of 30 cm and an aspect ratio less than five. This test series and series “a” only differed in bedform entrance and exit slope angles.

It is assumed that there is no obstacle or vegetation cover in the flow, and the flume width is constant. Additionally, the selected reaches in the river have negligible variation in plan and the selected reaches, and the flow is non-uniform due to the pool-riffle sequence.

### 2.3. Quadrant Analysis

The quadrant analysis is used to conditionally sample velocity time series to find out the role of each quadrant (outward, ejection, inward and sweep) on Reynolds stress. This study has also analyzed field investigations in the Pelasjan River in Iran and compared the results with laboratory ones. One of the goals of this research was to study the implications of pool and riffle bedforms on turbulent flow structures. The theoretical foundations of bursting provide a tool for better understanding this issue. The sequence of the bursting phenomenon is explained by two critical interactions of ejection and sweep. According to Figure 4, bursting occurs when a low-velocity flow streak with three-dimensional oscillation moves upward and away from the bed. The result of this process is called the ejection interaction, which is a low-velocity flow entering a turbulent flow. In the effect of ejection interactions, the separated flow becomes enlarged and retains its cohesive nature while being transmitted slowly in the direction of the flow. This step takes place in a short period, but eventually, its cohesive structure collapses, as shown in Figure 4c. Finally, as shown in Figure 4d, it is driven to the bed by a stream of water traveling rapidly. In other words, part of the fluid mass from the cohesive structure moves into the area adjacent to the bed and is distributed transversally, and this process is called sweep interaction. During the sweep interaction, the flow moves downstream, creating a thin shear layer with high oscillations and multiple vortices. Eventually, the adjacent flow lines merge, and the flow velocity decreases; thus, a low-velocity stream is formed near the bed again. This process is entirely a statistical analysis and cannot be observed physically. The strength and weakness of these velocity fluctuations and interactions demonstrate the degree of aggregation. These fluctuations are in the direction and perpendicular to the flow’s direction ( $u'$  and  $w'$ ) in each quadrant of quadrant analysis [24,25].

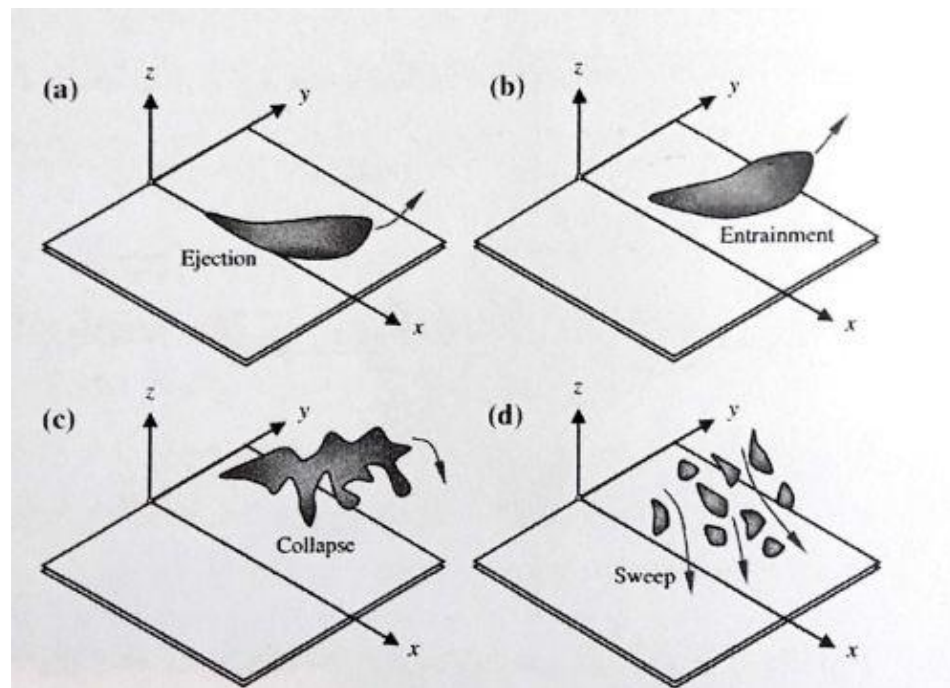


**Figure 4.** The bursting sequence of events including: (a) the beginning of stream streaks separation with the low-velocity flow (ejection), (b) the movement of the separated flow into the upper layer flow (except the low-velocity flow), (c) the collapse of the separated flow (except for low-velocity flow), and (d) moving of high-velocity stream streaks into the bed (sweep).

Traditionally, to evaluate the Reynolds shear stress  $-\rho \overline{u'v'}$  at a given point and to determine the contribution of each bursting interaction, the fluctuations of velocity components are plotted according to Figure 5 on a diagram with a longitudinal axis  $u'$  and a transverse axis  $w'$ . As shown in Figure 5, the shadow hyperbolic region surrounded by the curve  $|u'v'| = \text{constant}$  is known as a hole [26].

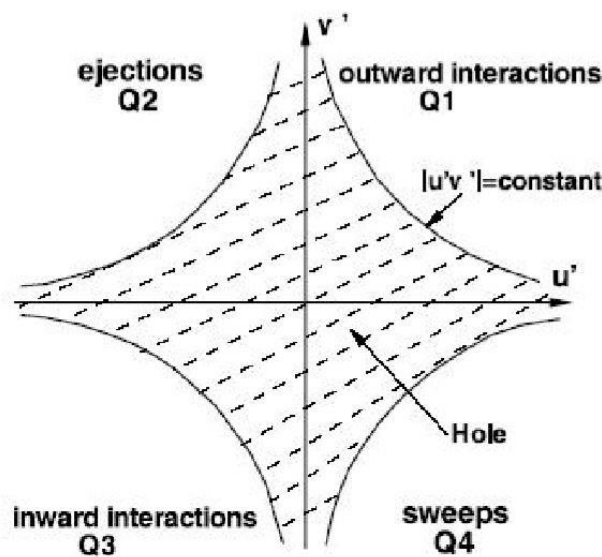


**Figure 5.** The four regions of interaction and the characteristics of the fluctuation.

### 3. Results

#### 3.1. Field Results

##### 3.1.1. The Velocity Profile in Pelasjan River

Figure 6 presents dimensionless velocity profiles along the river. The velocity profiles in the pool section are deformed with increasing water depth and decelerating flow, showing S-shaped distributions.

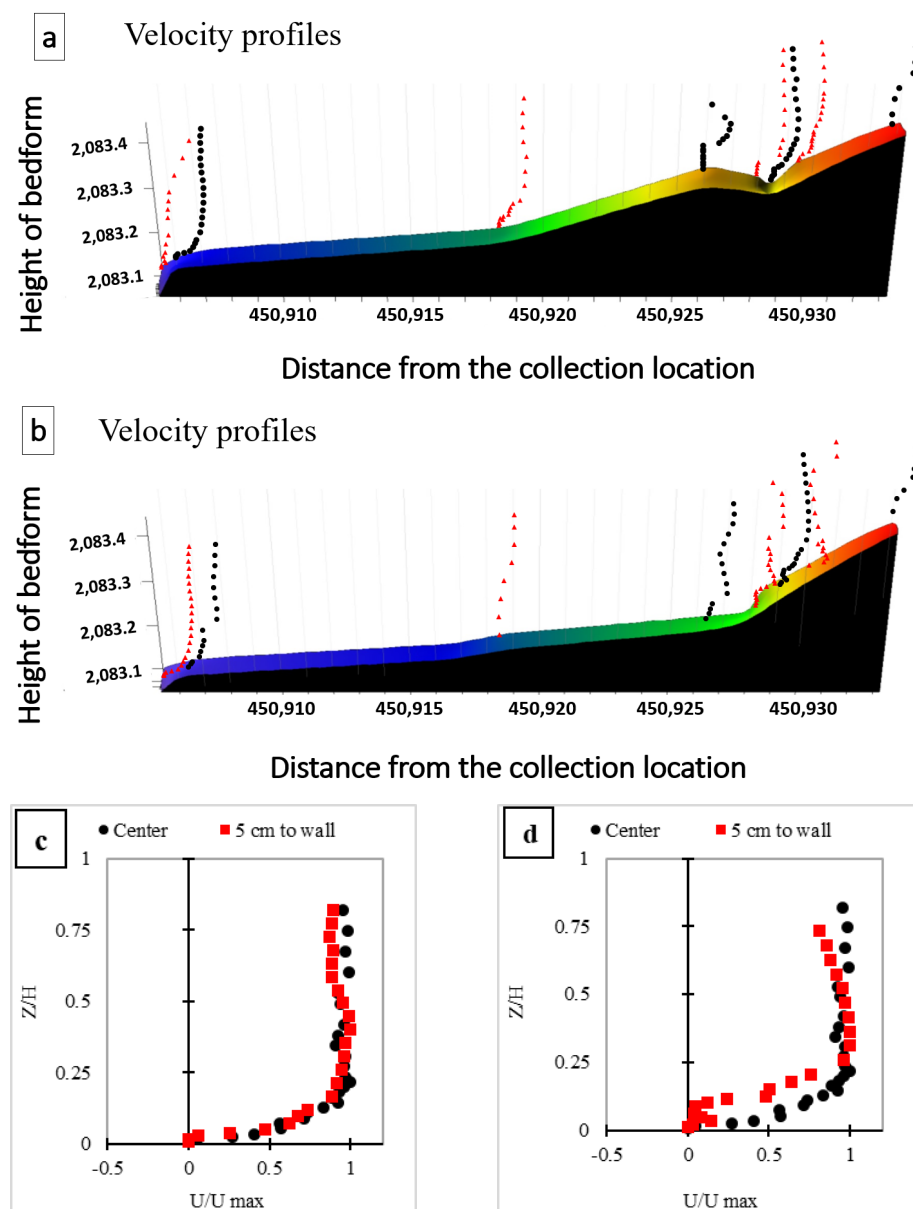


**Figure 6.** (a) Nondimensional velocity profiles ( $\frac{u}{U_{max}}$ ) in the longitudinal direction and at 5 cm of the left bank of the river, (b) nondimensional velocity profiles in the central axis of the river, (c) velocity profiles for the pool entrance (CS3), and (d) velocity profiles for riffle area in the central and 5 cm from the riverbank (CS4).

The velocity profiles near the left bank (Figure 6a) are less regular than those in the central axis, especially at the end of the reach. The difference is due to the vegetation effect and changes in bed form geometry (the black color). Application of ADV is not easy near the wall and the bed. However, Figure 6a shows possible separation in velocity profiles for 5 cm to the wall. In fact, a complex internal boundary layer is formed near the wall, leading to more irregular velocity profiles in Figure 6a. The velocity profile in Figure 6d

shows that the maximum velocity occurs in  $\frac{z}{H} = 0.25$  for the case of 5 cm to the wall, which is due to the secondary current formation in the presence of vegetation on the wall. Figure 6c shows the velocity profiles for the pool section in the flow direction in the central axes and 5 cm away from the left bank of the river. According to the figure, the maximum velocity occurred at  $0.2 < \frac{z}{H} < 0.5$ . In the pool section, the profiles close to the bank at 5 cm are similar to the velocity profiles in the center, indicating that the velocity profiles are not influenced by approaching the riverbank. Figure 6d shows that, in the riffle area, the average velocity decreases from the central axis toward the bank, meaning that the bank vegetation plays a more significant role in the flow velocity in the riffle area than in the pool. Additionally, the velocity distribution shows a parabolic shape in the riffle area of the central region, and maximum velocity occurs at  $0.2 < \frac{z}{H} < 0.4$ .

### 3.1.2. Reynolds Stress Profiles

Figure 7a shows the Reynolds stress profiles at 5 cm from the left bank of the river and on the central axis of the river (Figure 7b). For a better comparison between profiles, and to normalize Reynolds stress profiles, shear stress ( $U^*$ ) calculated from the boundary layer method was used.

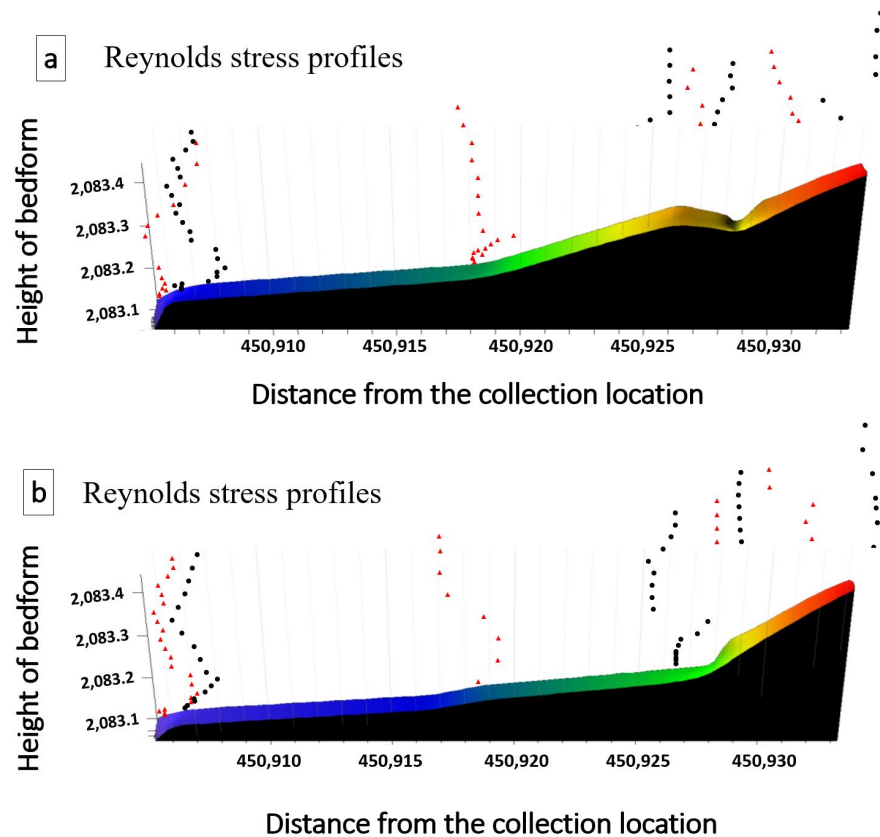


**Figure 7.** Nondimensional Reynolds stress profiles ( $\frac{-U'W'}{U_*^2}$ ) in the longitudinal direction at: (a) 5 cm of the left bank of the river, and (b) the central axis of the river.

According to Figure 8a, at a distance of 5 cm from the riverbank in the pool area, the Reynolds stress values are low, close to zero, and then become negative. The maximum Reynolds stress occurs at  $\frac{z}{H} = 0.2$ , and closer to the water surface, it plummets to negative values. Moving away from the riverbank means the maximum Reynolds stress occurs in the central axis at  $0.2 < \frac{z}{H} < 0.4$ . In Figure 8b, while Reynolds stress near the bank is higher than the central profile in the riffle area, in the central axis, the Reynolds stress starts from negative and rises to positive values as it approaches the water surface. Near the bank, however, the Reynolds stress values increased positively from the beginning, then they declined and again became positive near the surface. This complex distribution

of Reynolds stress is due to the interaction of the three-dimensional pool-riffle with the three-dimensional flow and the influence of other uncontrollable factors.

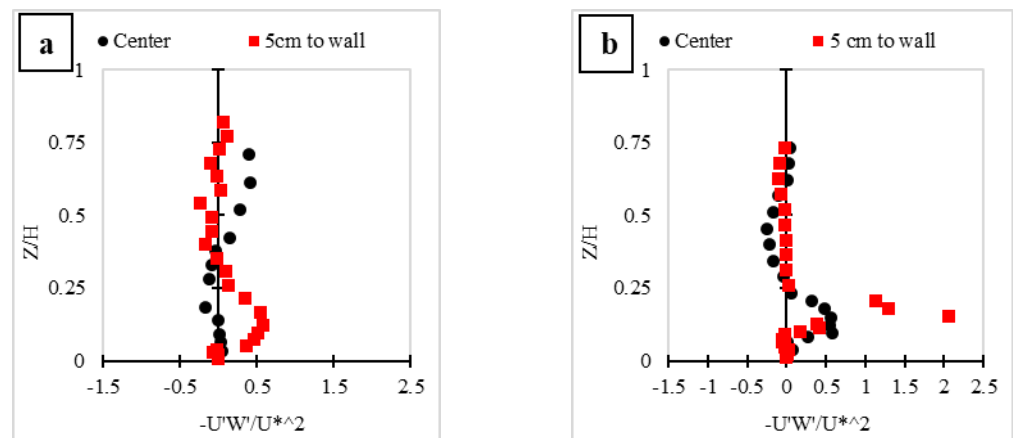


**Figure 8.** Reynolds stress profiles for: (a) the pool area and (b) the riffle area in the center and 5 cm from the riverbank.

### 3.1.3. Quadrant Analysis

Figure 9 shows the results of quadrant analysis at the pool and riffle zones in the central axis of the river. According to the Figure, the predominant event in the pool area is sweep, especially at  $\frac{Z}{H} = 0.1$ . This event is due to unfavorable pressure gradients and more turbulence from the separation zone in the pool area. By approaching the water surface and decreasing the effect of turbulence, the contribution of sweep decreases, and the outward event gradually becomes the dominant event. The ejection also plays a significant role in the riffle zone near the bed at  $\frac{Z}{H} = 0.2$ . However, inward and outward events are predominant near the water surface, indicating less turbulence in this zone compared to the pool zone.

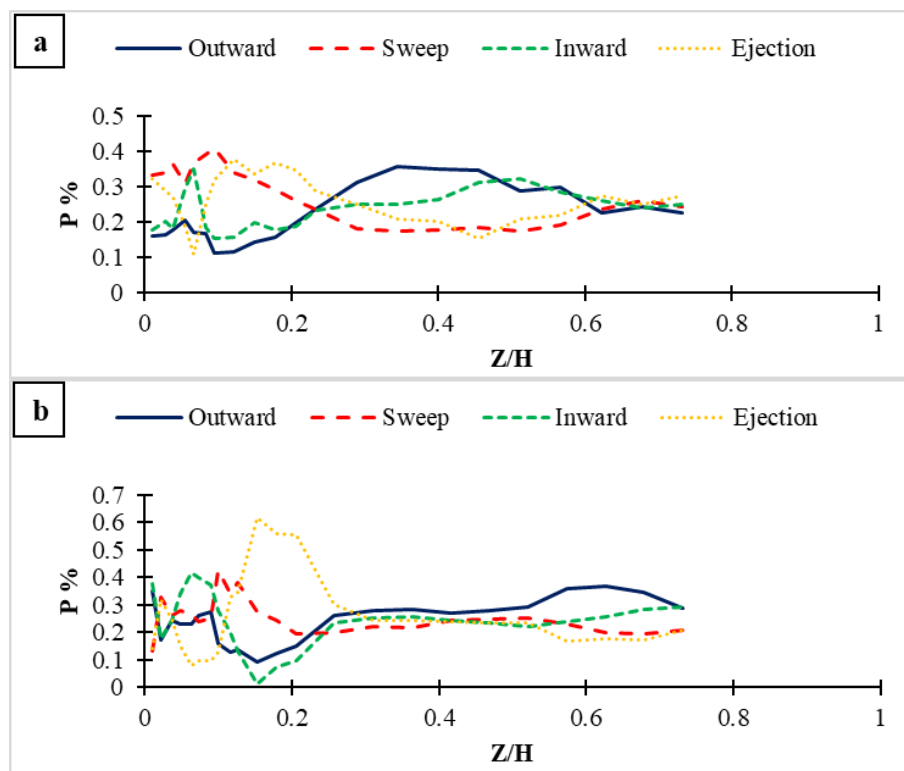


**Figure 9.** Contribution of each event in the central axis of the river in: (a) the pool and (b) the riffle.

### 3.2. Laboratory Results

#### 3.2.1. Velocity Profiles

The velocity contours in Figure 10a represent the velocity along the central axis of the flow. Accordingly, approaching the water surface and passing through the shear layer, the velocity becomes almost uniform, since the effect of bedform on the flow velocity decreases. Figure 10b shows the velocity contour in the selected reach in the x-direction for experiment series “b”. Based on the velocity contour on the bedform, the maximum velocity occurs near the water surface in the center of the flume, and no negative velocity values were observed. The outcomes are consistent with other researchers’ results [3,11,12,27]. Figure 10c shows x-direction velocity (cm/s) contours in the center of the flume for an angle of 20° with an aspect ratio of three (series “c”). Dark blue points in the pool area and downstream from the crest bedform indicate a negative velocity near the bed, showing the momentum loss region. The figure shows that the velocity reached  $-4$  cm/s, and the velocity reversal resulted from a decrease in momentum loss near the bed. Unfavorable pressure gradients are one of the causes; as the pressure gradient increases, the kinetic energy of the water decreases, changing the water direction and causing negative velocity vectors to appear near the bed. According to Figure 10c, the flow separation zone in the central axis of the channel occurred after the entrance slope from 8.25 m to 9 m. The approximate length of the separation zone was 0.75 m, which is equivalent to 4.1 of the bedform’s crown height, showing a good agreement with other studies [3,10,12,28].

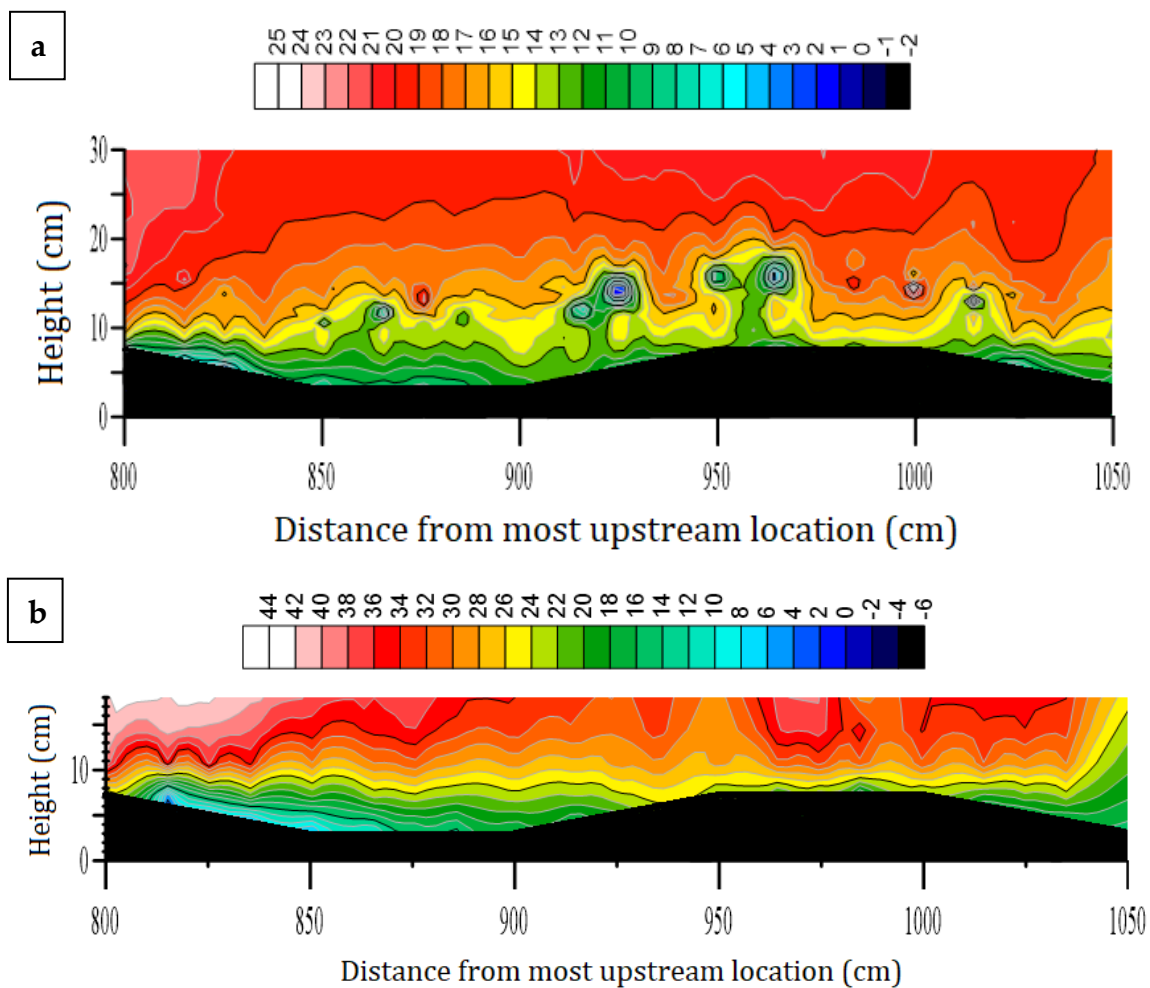
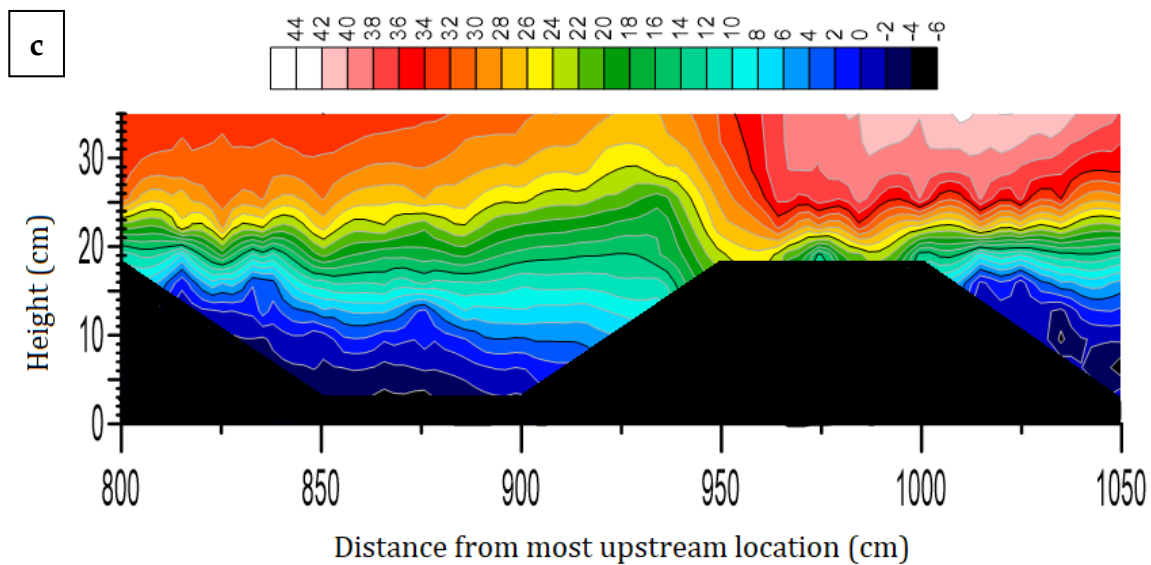
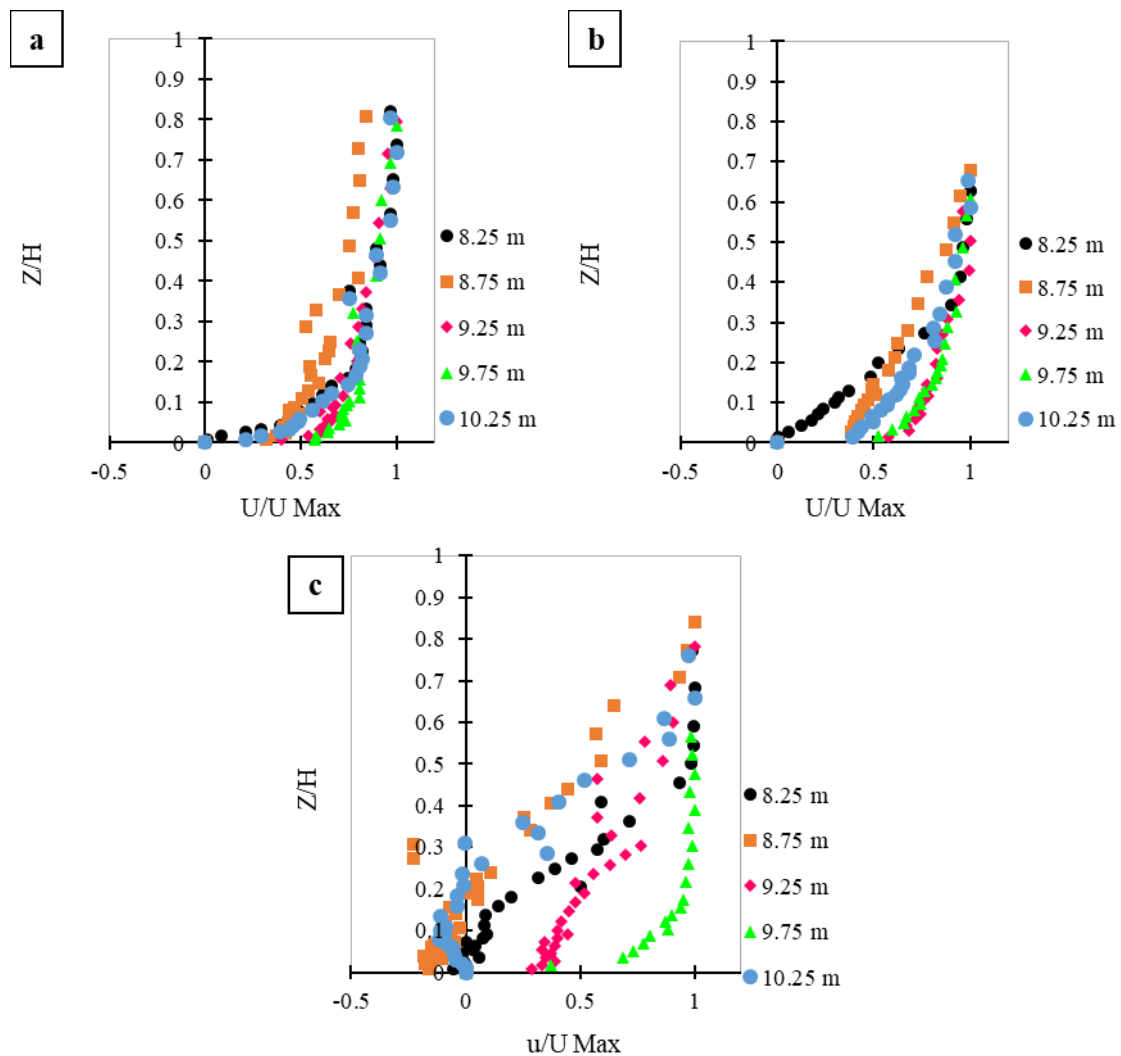


Figure 10. Cont.



**Figure 10.** Velocity contour in the x-direction for: (a) series “a” test in the central axis of the channel, with an angle of  $5^\circ$  and aspect ratio of less than five, (b) series “b” test in the center axis of the flume, with an angle of  $5^\circ$  and aspect ratio of more than five, and (c) series “c” test in the center axis of the flume, with an angle of  $20^\circ$  and an aspect ratio of less than five.

In addition, Figure 11a shows that the maximum velocity occurs at  $x = 9.75$  m and  $x = 9.25$  m in the riffle zone, and the minimum velocity occurs at the beginning of the bed entrance area in the pool zone in series “a”. There was no uniform flow in the middle part, which is similar to the finding of [5], and in the middle part of the riffle section, the flow uniformity did not occur due to the residual effect of the entrance slope [8]. Figure 11b compares the velocity profiles in five sections in more detail. The profiles are taken in 8.25 m, 8.75 m, 9.25 m, 9.75 m, and 10.25 m, in the entrance slope of the pool area, the flat surface of the bedform, the exit slope of the pool section (the entrance slope of riffle area), the crest of the riffle, and the exit slope of the riffle, respectively. Figure 11 shows that the velocity profiles in the riffle and pool areas tend to increase. The cause of this phenomenon can be attributed to the low slope angle and insignificant effects of the bedform on the flow. The velocity gradient in the pool part is greater than the middle part and the riffle section of the bedform, and the middle part experiences a more significant velocity gradient than the riffle section, which reinforces the results obtained by [11]. According to Figure 11c, the velocity profile has an increasing trend, and the maximum velocity occurs near the water surface. The velocity profile is divided into three zones downstream of the reattachment point [27]. In the first zone ( $\frac{z}{H} \ll 0.1$ ), the internal boundary layer is forming; in the second zone ( $0.1 < \frac{z}{H} < 0.5$ ), there is convection and diffusion of the mixing layer; and, in the third zone ( $0.5 < \frac{z}{H}$ ), the flow is not affected by the bedform. These results show that the pool-riffle sequence plays a significant role in the flow structure and velocity distribution.



**Figure 11.** Velocity profiles for: (a) series “a” test on the central axis of the channel with an angle of  $5^\circ$  and aspect ratio of less than five, (b) series “b” test on the central axis of the flume with an angle of  $5^\circ$  and aspect ratio of more than five, and (c) series “c” test on the central axis of the flume with an angle of  $20^\circ$  and aspect ratio of less than five. In the experiments with angles of  $20^\circ$ , in the pool area ( $x = 8.25$  m and  $x = 8.75$  m), the maximum velocity occurs at  $\frac{Z}{H} = 0.25$ , and in the riffle area ( $x = 9.25$  m), the maximum velocity was observed at  $\frac{Z}{H} = 0.4$ .

### 3.2.2. Reynolds Stress Profiles

Figure 12a shows the Reynolds stress distribution along the selected reach. Many researchers reported such Reynolds stress patterns in bedforms [3,10,12,24]. The Reynolds stress profiles in the central axis of the channel in the direction of the flow present some differences near the bed, but, when approaching the water surface, a decreasing trend is observed. The form of Reynolds stress distribution can be attributed to the interaction of the bedform–longitudinal pressure gradient and internal boundary layer, which starts from the end of the pool and finishes at the crest of the riffle. Some researchers have divided the shear stress distribution into three areas [11]. The first zone, which is closest to the bed, has a Reynolds stress profile that starts from a non-zero value with an upward trend to the water surface, reaching its maximum value at the border between the first and second zones. The second zone of the Reynolds stress profile takes a downward trend and reaches its minimum value of zero at the border of the second and third zones. In the third zone, Reynolds stress values were close to zero, which may not be studied due to the limitations of the ADV device near the water surface [11]. The results of Reynolds stress profiles in

Figure 9a are consistent with the results reported by [29,30]. Based on Figure 12b, Reynolds stress profiles do not follow a specific pattern. In  $x = 8.25$  m, 8.75 m, and 10.25 m, where the flow decelerates, profiles have riffle shapes. The observations in this area are consistent with previous research on the decelerating flow in a pool [3,31,32]. Figure 12c shows a riffle distribution with a turning point in each profile. Reynolds stress values increase from the bed to the turning point and then decline toward the water surface.

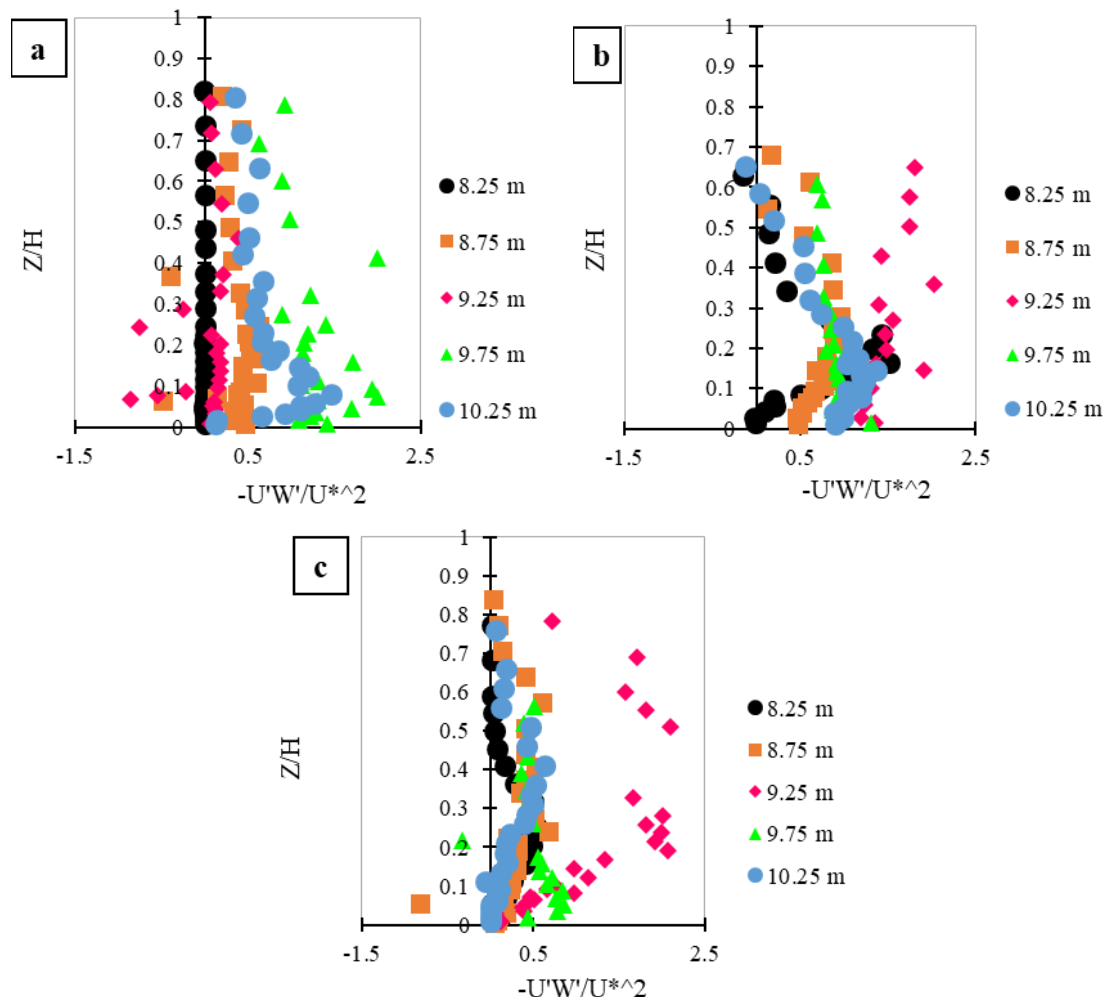


**Figure 12.** Reynolds stress profiles for: (a) series “a” test on the central axis of the channel with an angle of  $5^\circ$  and aspect ratio of less than five, (b) series “b” test on the central axis of the flume with an angle of  $5^\circ$  and aspect ratio of more than five, and (c) series “c” test on the central axis of the flume with an angle of  $20^\circ$  and an aspect ratio of less than five.

### 3.2.3. Quadrant Analysis

Figure 13 shows the quadrant analysis performed for all points of a Reynolds stress profile in four areas: the pool entrance, the middle of the pool, the riffle, and the crest of the riffle. The results show that ejection dominates in each profile at approximately  $\frac{Z}{H} = 0.2$  and near the bed for all four areas in series “a”. In contrast, for  $\frac{Z}{H} > 0.2$ , the outward event is dominant. In Figure 13b, the predominant event in the pool area up to  $\frac{Z}{H} < 0.2$  is the ejection, indicating a vortex motion near the bed, resulting in a positive Reynolds stress. For  $\frac{Z}{H} > 0.2$ , the outward event is dominant, showing a reduction of turbulence in this region. The same trend continues in the middle of the pool due to the effect of flow slowing down and quasi-uniform flow. In the riffle area and on the crest, the dominant event is outward. For the quasi-uniform flow in the middle of the pool and the entrance of the riffle area, the first dominant event is outward.

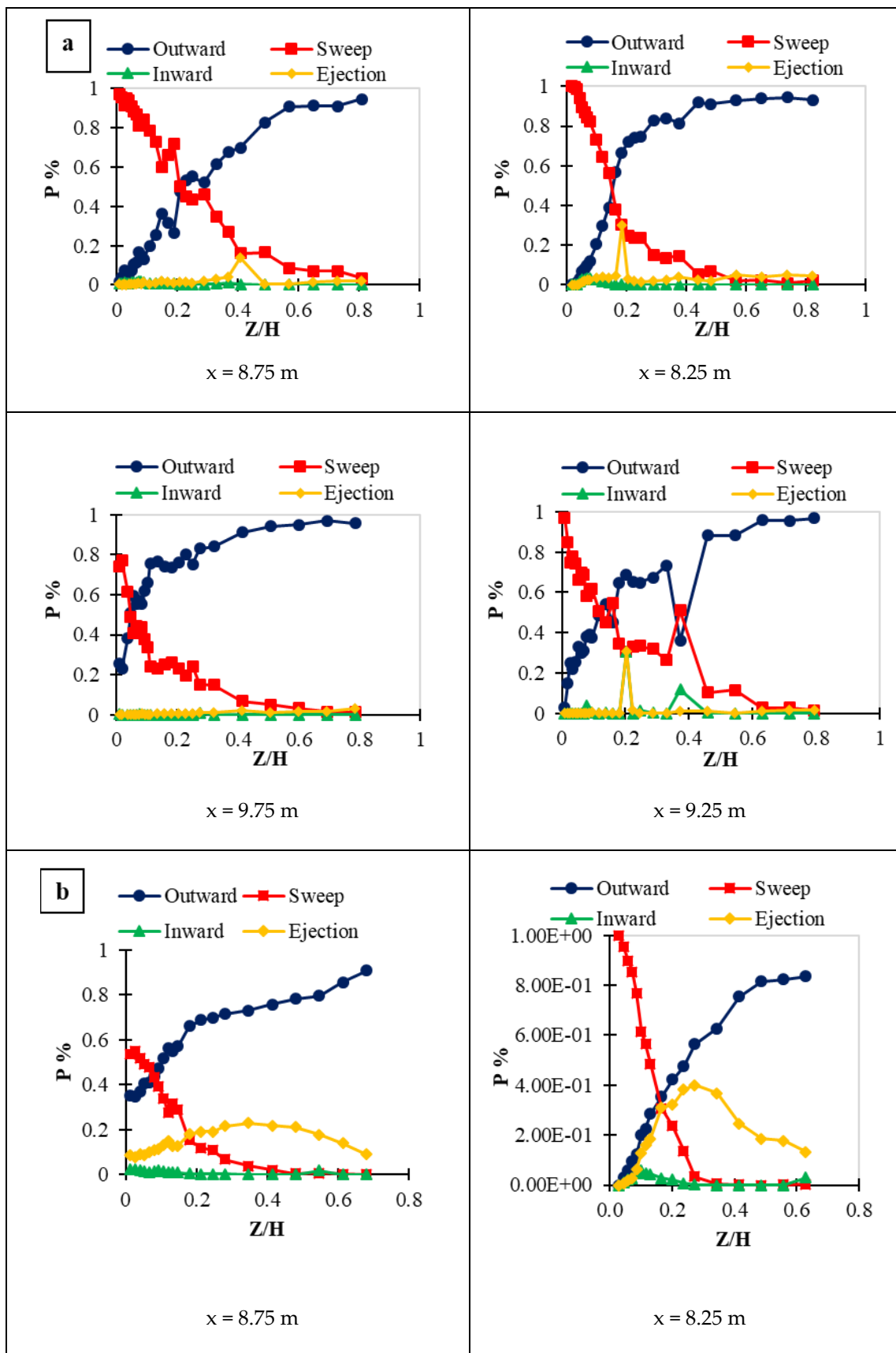
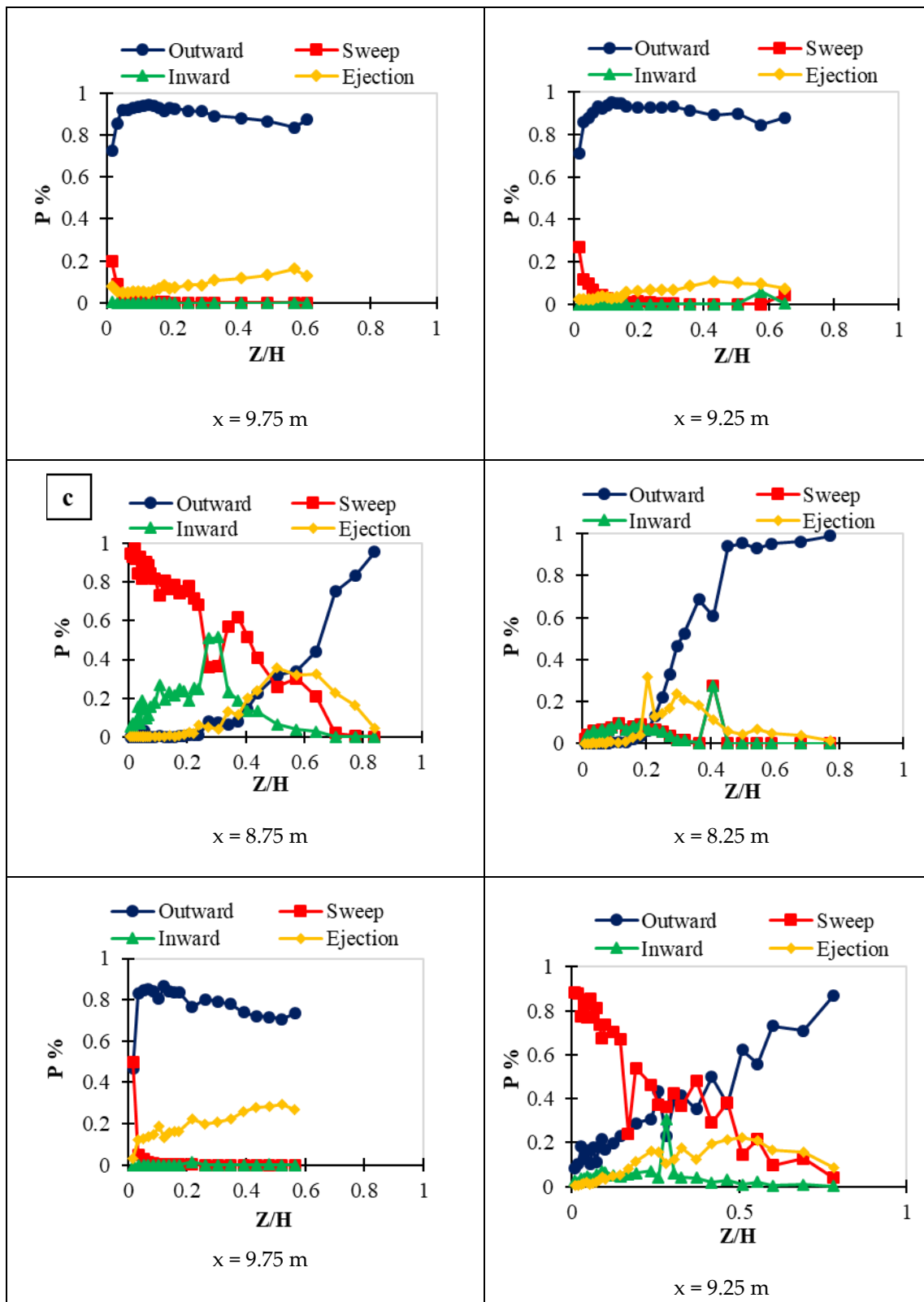


Figure 13. Cont.



**Figure 13.** Dominant interactions using quadrant analysis for: (a) series “a” test on the central axis of the channel, with an angle of  $5^\circ$  and aspect ratio of less than five, (b) series “b” test on the central axis of the flume, with an angle of  $5^\circ$  and aspect ratio of more than five, and (c) series “c” test on the central axis of the flume with an angle of  $20^\circ$  and aspect ratio of less than five.

#### 4. Discussion

As mentioned above, there are no specific criteria to apply laboratory results to rivers. The comparison of velocity distributions (Figures 6b and 11) shows that there is no inflection point in the flume and the central axis of the river. This nearly similar distribution in the river and laboratory can help to extend the applications of velocity profile, including the estimation of bed shear stress for one-dimensional flows by different methods, such as the log law. Additionally, a similar pattern in Reynolds stress distributions (Figures 7b and 12) in the central axis of the river and laboratory are good because many details may be collected in the laboratory and extend to rivers. The convex distribution of Reynolds stress in both field and laboratory can be explained by the momentum equation. The increasing longitudinal pressure gradient near the bed leads to increasing vertical distribution of Reynolds stress, as it is observed in Figures 7b and 12 by a convex form. This similarity can help to better determine the key fluvial hydraulic parameters in rivers by application of the momentum equation. It should be noted that the exact modeling of gravel-bed rivers on a laboratory scale is a difficult task. For example, accurate topographical survey, grain size, and bed form variations may not be easily modeled, demanding significant simplifications of the complex conditions in a river to work under controlled laboratory conditions.

The results of velocity and Reynolds stress distributions over an artificial pool-riffle sequence show a reasonable agreement with a natural pool-riffle in a gravel-bed river. This achievement can be used by other researchers to decrease field costs and to better investigate the flow details on a laboratory scale extending the results to rivers. It is observed that by increasing the entrance slope of the pool, the flow velocity profiles show negative values, the flow separation due to the unfavorable pressure gradient, and the development of reverse flow. However, the flow separation is not observed for the mild entrance slope of the pool ( $5^\circ$ ). By comparing the Reynolds stress results in the artificial and natural pools and riffles, it was found that the distribution of Reynolds stress is due to the interaction of the complex behavior of the pool-riffle sequence with the three-dimensional flow and the influence of other uncontrollable factors in rivers. However, this Reynolds stress distribution can be attributed to the interaction of the bedform, longitudinal pressure gradient, and the internal boundary layer in the artificial channel. In the  $5^\circ$  entrance slope of the pool where the flow decelerates, the Reynolds stress profiles display convex distribution in general.

Velocity contours show that the velocity gradient increases with an increasing entrance slope, which is consistent with the results of previous studies [3,11]. The minimum velocity occurs in the pool entrance and the flat part. As the entrance slope increases to  $20^\circ$ , the minimum velocity value decreases, leading to the generation of negative velocity in this slope. The Reynolds stress distributions reveal that by increasing the entrance slope of the pool, the maximum Reynolds stress is formed due to decelerating flow and a change in the Reynolds stress sign, indicating the occurrence of flow separation in the pool entrance at the  $20^\circ$  slope angle. Additionally, the slope angle directly affects the length of the flow separation zone and the shape of the Reynolds stress distribution.

A comparison of quadrant analysis for an artificial and natural pool-riffle sequence shows that the trend of decreasing sweep and increasing outward events from near the bed toward the water surface is almost similar. This means that the dominant events of the bursting process are independent of the scale effect. In fact, despite complex three-dimensional flow and geometry in a river, an artificial pool-riffle sequence in a laboratory can reach similar results.

The change in aspect ratio ( $w/h$ ) for a constant entrance slope causes a considerable change in the contribution of different events in the bursting process. This is especially significant for sweep contribution in the riffle area. For a large aspect ratio ( $w/h > 5$ ), where the flow is considered two-dimensional, the contribution of sweep decreases near the bed but the contribution of ejection increases. However, for a small aspect ratio ( $w/h < 5$ ), where the flow in a straight flume is considered three-dimensional, the sweep role is dominant near the bed, which can enhance the sediment transport processes.

## 5. Conclusions

Similar velocity and Reynolds stress distributions between an artificial pool-riffle in the laboratory with a natural one in a gravel-bed river were observed in this study. Additionally, the application of ADV as an affordable measuring tool was found to be promising to observe similar patterns in turbulence features in both conditions of laboratory and river. For a mild entrance slope of  $5^\circ$  (Figure 11a,b), no inflection point was observed. However, for a steep entrance slope of  $20^\circ$ , from 825 m to 9.25 m, a clear inflection point was observed in each velocity profile (Figure 11c). Additionally, no inflection point in velocity distribution in the central axis of the river was observed (Figure 7b). The convex distributions of Reynolds stress in the river and laboratory showed similar results. These similarities between laboratory and river encourage researchers to better determine the key fluvial parameters of flow resistance and sediment transport.

This research investigated the velocity and Reynolds stress distributions in natural and artificial pool-riffle sequences. The field study was conducted in the Pelasjan River in central Iran, and the laboratory experiment was carried out in a rectangular flume. The results showed that no flow separation and no reverse sign of velocity were observed at the pool entrance for the  $5^\circ$  slope. However, the flow separation was observed by increasing the entrance slope of the pool to  $20^\circ$ . When the entrance slope was  $5^\circ$ , the velocity profiles presented an exponential trend, but for the entrance slope of  $20^\circ$ , the profiles displayed a S-shaped pattern. It was concluded that variation of entrance slope does not influence the convex shape of Reynolds stress distribution, but it influences the location of the maximum value of the Reynolds stress and the length of the flow separation zone.

Quadrant analysis showed that the dominant events were outward and ejection in the pool-riffle sequence for both field and laboratory settings. The sweep event presented a decreasing trend from near the bed toward the water surface. However, an increasing trend was observed for the outward event from the bed toward the water surface. The results of this research show that velocity, Reynolds stress, and dominant events of the bursting process can be investigated under controlled conditions in the laboratory and extend to complex conditions in rivers.

For small aspect ratios ( $w/h < 5$ ), the contribution of sweep near the bed was dominant, but for  $w/h > 5$ , the contribution of sweep decreased significantly, while the role ejection increased.

The results of this study are encouraging because they showed a reasonable agreement between the field and laboratory findings. This can help to plan and to design the fluvial processes under control conditions and extend the results to the rivers with less cost and more details.

**Author Contributions:** Conceptualization, H.A.; methodology, H.A.; software, N.S., H.A., E.S.T., A.E. and M.K. (Marzieh Khabari); validation, H.A. and M.N.-S.; resources, H.A., M.N.-S. and M.K. (Marzieh Khabari); data curation, N.S., H.A., E.S.T. and A.E.; writing—original draft preparation, N.S., H.A., E.S.T. and M.N.-S.; writing—review and editing, N.S., H.A., E.S.T. and M.N.-S.; visualization, N.S., H.A., E.S.T. and A.E.; supervision, H.A., M.N.-S. and M.K. (Moses Karakouzian); project administration, H.A.; All authors have read and agreed to the published version of the manuscript.

**Funding:** This research received no external funding.

**Data Availability Statement:** The data are available upon request.

**Conflicts of Interest:** The authors declare no conflict of interest.

## References

1. Ataollahi, N.; Khabari, M.; Tabarestani, E.S.; Singh, V.P.; Afzalimehr, H. Interaction of Three-Dimensional Pool-Riffle Sequence and the Flow Characteristics in the Presence of Wall Vegetation. *J. Civ. Eng. Res.* **2001**, *11*, 51–61.
2. Dodangeh, E.; Afzalimehr, H. Incipient motion of sediment particles in the presence of bed forms under decelerating and accelerating flows. *J. Hydrol. Hydromech.* **2022**, *70*, 89–102. [[CrossRef](#)]
3. Fazlollahi, A.; Afzalimehr, H.; Sui, J. Effect of slope angle of an artificial pool on distributions of turbulence. *Int. J. Sediment Res.* **2015**, *30*, 93–99. [[CrossRef](#)]

4. Hassan, M.A.; Radić, V.; Buckrell, E.; Chartrand, S.M.; McDowell, C. Pool-riffle adjustment due to changes in flow and sediment supply. *Water Resour. Res.* **2001**, *57*, e2020WR028048. [[CrossRef](#)]
5. MacVicar, B.; Roy, A. Hydrodynamics of a forced riffle pool in a gravel bed river: 1. Mean velocity and turbulence intensity. *Water Resour. Res.* **2007**, *43*, W12401. [[CrossRef](#)]
6. Nabaei, S.F.; Afzalimehr, H.; Sui, J.; Kumar, B.; Nabaei, S.H. Investigation of the Effect of Vegetation on Flow Structures and Turbulence Anisotropy around Semi-Elliptical Abutment. *Water* **2021**, *13*, 3108. [[CrossRef](#)]
7. Thompson, D.M. The characteristics of turbulence in a shear zone downstream of a channel constriction in a coarse-grained forced pool. *Geomorphology* **2007**, *83*, 199–214. [[CrossRef](#)]
8. MacVicar, B.; Roy, A. Hydrodynamics of a forced riffle pool in a gravel bed river: 2. Scale and structure of coherent turbulent events. *Water Resour. Res.* **2007**, *43*. [[CrossRef](#)]
9. MacVicar, B.J.; Obach, L.; Best, J.L. Large-scale coherent flow structures in alluvial pools. In *Coherent Flow Structures at Earth's Surface*; Wiley Online Library: New York, NY, USA, 2013; pp. 243–259.
10. Motamedi, A.; Afzalimehr, H.; Singh, V.P.; Dufresne, L. Experimental study on the influence of dune dimensions on flow separation. *J. Hydrol. Eng.* **2014**, *19*, 78–86. [[CrossRef](#)]
11. Najafabadi, E.F.; Afzalimehr, H.; Rowiński, P.M. Flow structure through a fluvial pool-riffle sequence—Case study. *J. Hydro-Environ. Res.* **2018**, *19*, 1–15. [[CrossRef](#)]
12. MacVicar, B.J.; Rennie, C.D. Flow and turbulence redistribution in a straight artificial pool. *Water Resour. Res.* **2012**, *48*. [[CrossRef](#)]
13. MacVicar, B.; Obach, L. Shear stress and hydrodynamic recovery over bedforms of different lengths in a straight channel. *J. Hydraul. Eng.* **2015**, *141*, 04015025. [[CrossRef](#)]
14. Rayburg, S.C. *Three Dimensional Morphologic and Hydraulic Characteristics of Pools, Riffles and Pool-Riffle Sequences*; State University of New York: Buffalo, NY, USA, 2005.
15. Caamaño, D.; Goodwin, P.; Buffington, J. Flow structure through pool-riffle sequences and a conceptual model for their sustainability in gravel-bed rivers. *River Res. Appl.* **2012**, *28*, 377–389. [[CrossRef](#)]
16. Soltani, N.; Afzalimehr, H.; Singh, V.P. Influence of Vegetated Banks on Turbulent Characteristics of Non-uniform Flow in Gravel Bed River. *Int. J. Hydraul. Eng.* **2020**, *9*, 15–23.
17. Afzalimehr, H.; Barahimi, M.; Sui, J. Non-uniform flow over cobble bed with submerged vegetation strip. In *Proceedings of the Institution of Civil Engineers-Water Management*, ICE Publishing, London, England; 2019; 172, pp. 86–101.
18. Cooper, J.R.; Aberle, J.; Koll, K.; Tait, S.J. Influence of relative submergence on spatial variance and form-induced stress of gravel-bed flows. *Water Resour. Res.* **2013**, *49*, 5765–5777. [[CrossRef](#)]
19. McSherry, R.; Chua, K.; Stoesser, T.; Mulahasan, S. Free surface flow over square bars at intermediate relative submergence. *J. Hydraul. Res.* **2018**, *56*, 825–843. [[CrossRef](#)]
20. Leopold, L.B.; Wolman, M.G.; Miller, J.P.; Wohl, E. *Fluvial Processes in Geomorphology*; Courier Dover Publications: New York, NY, USA, 2020.
21. Kabiri, F.; Afzalimehr, H.; Sui, J. Flow structure over a wavy bed with vegetation cover. *Int. J. Sediment Res.* **2017**, *32*, 186–194. [[CrossRef](#)]
22. Nikora, V.I.; Goring, D.G. ADV measurements of turbulence: Can we improve their interpretation? *J. Hydraul. Eng.* **1998**, *124*, 630–634. [[CrossRef](#)]
23. Shahiri Tabarestani, E.; Afzalimehr, H.; Pham, Q.B. Validation of double averaged velocity method in a variable width river. *Earth Sci. Inform.* **2021**, *14*, 2265–2278. [[CrossRef](#)]
24. Dey, S. Sediment threshold. In *Fluvial Hydrodynamics*; Springer: Berlin/Heidelberg, Germany, 2014; pp. 189–259.
25. Head, M.; Bandyopadhyay, P. New aspects of turbulent boundary-layer structure. *J. Fluid Mech.* **1981**, *107*, 297–338. [[CrossRef](#)]
26. Nezu, I.; Nakagawa, H. *Turbulence in Open-Channel Flows*; Routledge: Oxfordshire, UK, 2017.
27. Bennett, S.; Best, J. Mean flow and turbulence structure over fixed, two-dimensional dunes: Implications for sediment transport and bedform stability. *Sedimentology* **1995**, *42*, 491–513. [[CrossRef](#)]
28. Nelson, J.M.; Smith, J.D. Mechanics of flow over ripples and dunes. *J. Geophys. Res. Ocean.* **1989**, *94*, 8146–8162. [[CrossRef](#)]
29. Afzalimehr, H.; Subhasish, D. Influence of bank vegetation and gravel bed on velocity and Reynolds stress distributions. *Int. J. Sediment Res.* **2009**, *24*, 236–246. [[CrossRef](#)]
30. Yang, K.; Cao, S.; Knight, D.W. Flow patterns in compound channels with vegetated floodplains. *J. Hydraul. Eng.* **2007**, *133*, 148–159. [[CrossRef](#)]
31. Afzalimehr, H.; Anctil, F. Accelerating shear velocity in gravel-bed channels. *Hydrol. Sci. J.* **2000**, *45*, 113–124. [[CrossRef](#)]
32. Shahiri Tabarestani, E.; Afzalimehr, H.; Pham, Q.B. Flow structure investigation over a pool-riffle sequence in a variable width river. *Acta Geophysica* **2022**, *70*, 713–727. [[CrossRef](#)]

**Disclaimer/Publisher's Note:** The statements, opinions and data contained in all publications are solely those of the individual author(s) and contributor(s) and not of MDPI and/or the editor(s). MDPI and/or the editor(s) disclaim responsibility for any injury to people or property resulting from any ideas, methods, instructions or products referred to in the content.